Title

Electrochemical Therapy of In Vivo Rabbit Cutaneous Tissue

Journal

The Laryngoscope, 131(7)

ISSN

0023-852X

Authors

Hong, Ellen M

Pham, Tiffany T

Seo, Soohong

et al.

Publication Date

2021-07-01

DOI

10.1002/lary.29461

The Laryngoscope

Electrochemical Therapy of In Vivo Rabbit Cutaneous Tissue

Ellen M. Hong, BA; Tiffany T. Pham, MD; Soohong Seo, MD; Wesley J. Moy, PhD; Pamela Borden, BS; Kyle Hansen, BS; Sehwan Kim, PhD; Ji-Hun Mo, MD, PhD; Brian J. F. Wong, MD, PhD

Objectives: To examine the acid-base and histological changes in in vivo rabbit cutaneous tissue after electrochemical therapy.

Study Design: In vivo rabbit tissue study.

Methods: The shaved skin on the backs of female Oryctolagus cuniculi were assigned to treatments with or without tumescence with normal saline. Two platinum-needle electrodes were inserted into each treatment area and connected to a direct current (DC) power supply. Voltage (3–5 V) was varied and applied for 5 minutes. The wound-healing process was monitored via digital photography and ultrasonography until euthanasia at day 29. Treatment areas were biopsied, and specimens were sectioned through a sagittal midline across both electrode insertion sites. Samples were then evaluated utilizing light microscopy (hematoxylin and eosin, Masson's Trichrome, and Picrosirius red).

Results: Treatment sites developed mild inflammation that dissipated at lower voltages or became scabs at higher voltages. Ultrasonography demonstrated acoustic shadowing with spatial spread that increased with increasing voltage application. The 4- and 5-V sites treated with saline had localized areas of increased tissue density at day 29. Although specimens treated with 3 V did not look significantly different from control tissue, 4- and 5-V samples with and without saline tumescence had finer, less-organized collagen fibers and increased presence of fibrocytes and inflammatory infiltrates.

Conclusions: Electrochemical therapy caused localized injury to in vivo rabbit cutaneous tissue, prompting regenerative wound repair. With future development, this technology may offer precise, low-cost rejuvenation to restore the functionality and appearance of dermal scars and keloids.

Key Words: Electrochemical therapy, skin, scar revision, skin rejuvenation.

Level of Evidence: NA

***Laryngoscope*, 131:E2196–E2203, 2021**

INTRODUCTION

As the first line of defense, skin is subjected to senescent changes, photodamage, and injury among other challenges. The resultant scars and associated deformation may necessitate intervention to correct them. Conventional treatment for scars—including scar revision surgery, dermabrasion, steroid injections, pressure dressings, etc.—has highly variable efficacy. Contemporary minimally invasive treatments include pharmacologic agents, chemexfoliation, fractional laser ablation, and microneedling with and without radiofrequency.[1] However, these approaches can be difficult to optimize or control,[2] are often expensive, and often require multiple treatments.[3] For example, the efficacy of chemexfoliation is dependent on the depth of acid penetration, and the heterogeneous dermal landscape across the face causes variable results. Because the risk of scarring greatly increases with the depth of penetration, although expensive, chemical peels have been supplanted by lasers.[4] However, lasers have a superficial penetration of up to 900 microns, which is insufficient for treating the inherent depth of scars.[5] Although there are currently numerous treatments for dermal rejuvenation, there exists room for improvement and innovation.

Electrochemical therapy (ECT) is a potentially novel, low-cost alternative to treat scars. Initially, the effects of ECT were studied extensively in cartilage where *in situ* electrochemically generated pH gradients altered the static stress-strain profiles in cartilage to reshape it.[6–23] An incidental finding in these *in vivo* studies was the lack of injury to overlying skin despite contact with platinum electrodes that hydrolyzed tissue water to form an acid and base. Other than hair loss, there were no discernible visible skin changes. This observation motivates the present investigation focused on the isolated effects of ECT on skin remodeling. The application of an electrical potential within aqueous media (including skin) results in hydrolysis and the production of H+ and OH-, creating *in situ* pH gradients. Moy et al. examined ECT in *ex vivo* porcine skin, which produced localized pH gradients leading to collagen denaturation.[2] Hu et al. used nonlinear optical microscopy to identify changes in collagen structure in *ex vivo* human

From the Beckman Laser Institute & Medical Clinic (E.M.H., T.T.P., W.J.M., P.B., K.H., B.J.F.W.), University of California, Irvine, California, U.S.A.; Department of Dermatology (S.S.), Korea University Anam Hospital, Seoul, South Korea; Department of Biomedical Engineering, School of Medicine (S.K.), Dankook University, Cheonan, Republic of Korea; Beckman Laser Institute Korea (S.K., J.-H.M.), Dankook University, Cheonan-si, Chungnam, Republic of Korea; Department of Otorhinolaryngology, School of Medicine (J.-H.M.), Dankook University, Chenoan, Republic of Korea; Department of Biomedical Engineering (B.J.F.W.), University of California—Irvine, Irvine, California, U.S.A.; and the Department of Otolaryngology—Head and Neck Surgery (B.J.F.W.), University of California—Irvine, School of Medicine, Orange, California, U.S.A.

Editor's Note: This Manuscript was accepted for publication on February 6, 2021.

The authors declare no financial interests, activities, relationships, and affiliations with respect to this study.

Send correspondence to Brian J. F. Wong, MD, PhD, 1002 Health Sciences Road, Irvine, CA 92612. E-mail: bjwong@uci.edu

DOI: 10.1002/lary.29461

skin following the controlled application of ECT.[24] These studies established that, with ECT, voltage and application time are the principal components of dosimetry, and the region of tissue effect can be specified.

Although we have studied how ECT changes the matrix collagen structure in *ex vivo* skin, the dynamics of acute injury and subsequent wound-healing process triggered by ECT have not been investigated in vivo. This study is the first to examine the *in vivo* cutaneous effect of ECT in the New Zealand White rabbit model as a prelude to future potential therapeutic application.

MATERIALS AND METHODS

The study was approved by the University of California Irvine Institutional Animal Care and Use Committee (IACUC). Two female New Zealand White rabbits (*Oryctolagus cuniculus*) weighing 3.8 to 4.0 kg were treated with a subcutaneous dose of prophylactic antibiotic (enrofloxacin 5 mg/kg) and anesthetized with subcutaneous injections of ketamine hydrochloride (20–40 mg/kg) and xylazine hydrochloride (3-5 mg/kg). The back was shaved hairless, and individual ECT sites were demarcated with an ink pen. A custom acrylic jig was used to guide a single positive electrode (anode) and a single negative electrode (cathode) separated by 2 mm to establish an ECT site (Fig. 1). The first rabbit's skin was not tumesced with saline prior to ECT. The second rabbit underwent subcutaneous injection with 1.5 to 2 cc of normal saline solution until tumescence was achieved at each site immediately before performing ECT (Fig. 2A) to ease needle insertion and enhance electrolysis. Platinum-needle electrodes (0.3 mm in diameter; Grass Technologies) were used due to their high standard potential and minimal risk of electrode oxidation.[14,15,25–31] The electrode leads were connected to a DC power supply, and electrical potentials varying from 3 to 5 V were applied for 5 minutes to each site. A MATLAB program controlled the voltage and application time and monitored current.[14]

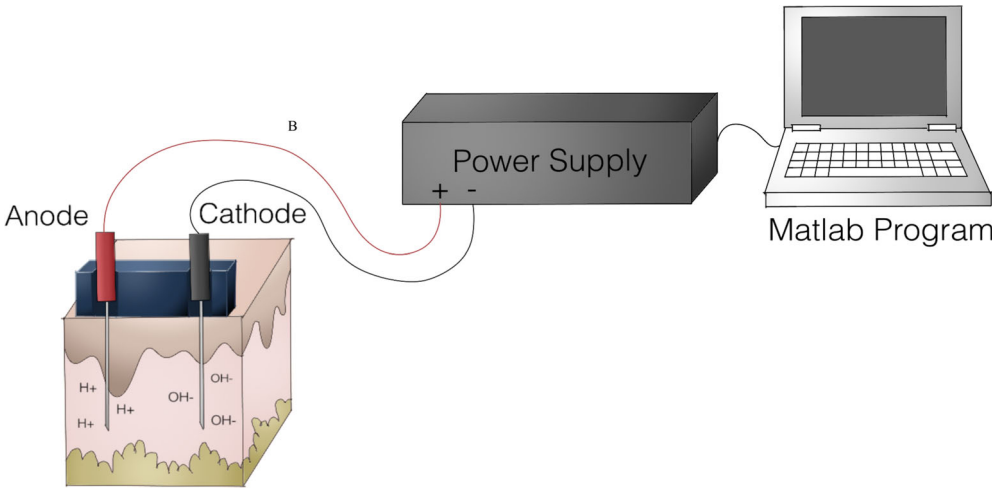

Fig. 1. Electrochemical therapy (ECT) mechanism and setup. Needle electrodes connected to a DC power supply are inserted into the skin 2 mm apart using an acrylic jig. The power supply's electrical potential and application time is controlled through a MATLAB program.

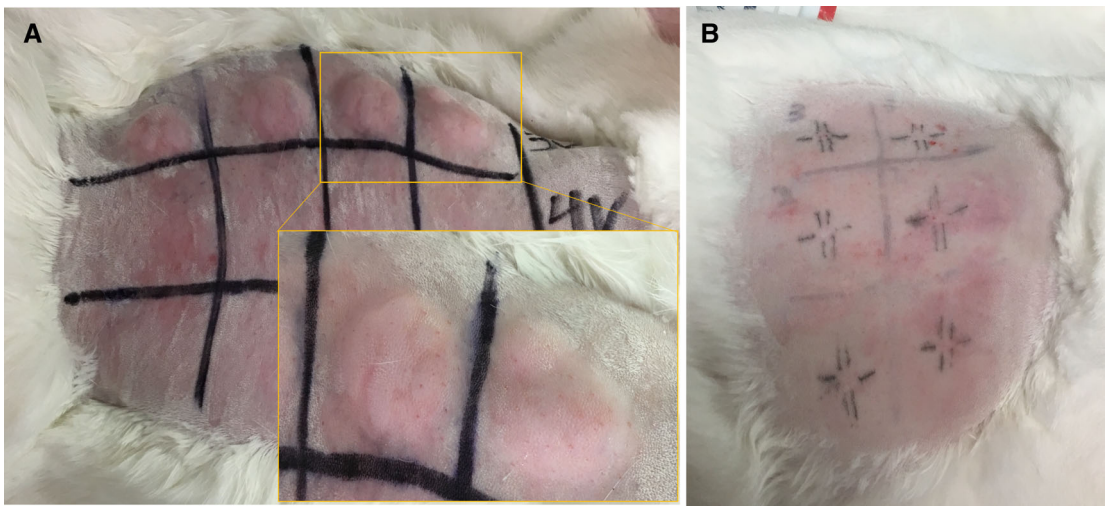

Fig. 2. Subcutaneous injection of saline. Rabbit dermal back tissue with (A) 2 cc subcutaneous saline injections and (B) tattooed registry marks.

Digital photography (Rebel XS; Canon) of the treatment sites and surrounding untreated areas were acquired before and after ECT. Ultrasound images (vertical resolution of 40 μm) were also acquired before and after treatment using a clinical high-frequency dermatologic ultrasonography system (Episcan I-200; Longport Inc). After ultrasonography, registry marks were tattooed, forming crosshairs at the electrode insertion site (Fig. 2B). Buprenorphine (0.01-0.05 mg/kg, IM) was injected subcutaneously every 12 hours for the first 24 hours for analgesia. Photography and ultrasound were performed on days 1, 7, 14, and 29. Prophylactic antibiotics were administered daily on days 1 to 3. Treatment sites were protected using an occlusal dressing (Tegaderm) after photography and ultrasound. Following experimental procedures on day 29, the animal was euthanized with intravenous administration of Euthasol (100 mg/kg). Immediately following euthanasia, ECT and control skin sites were excised (1 cm × 2 cm) and fixed in formalin for 1 week. The samples were processed,[32] and histological sections were stained with retrograde hematoxylin and eosin (H&E), Masson's Trichrome (MT), or Picrosirius red (PSR). MT staining provides elective staining of collagen, depending on structure permeability. Aniline blue staining is apparent on healthy collagen. Depending on the physical and physiochemical states of collagen fibers, denatured collagen is not stained by the aniline blue but instead by Biebrich Scarlet red.[33] PSR, when visualized with optically polarized light, differentiates between types I and III collagen.[34] Type I collagen appears as a red hue, whereas type III takes on a yellow-green color. Images of ECT and control sites were captured with visible light microscopy at 10× magnification.

RESULTS

Digital Photography

Photographs of ECT treatment sites were acquired on days 0,1, 7, 14, and 29 (Fig. 3). Control tissue was imaged on day 0 (Fig. 3A). Immediately after ECT application, procedure sites developed mild and localized inflammation—erythema and swelling—lingering for a week. The extent of inflammation increased with voltage. Tumescent regions where ECT was performed had more inflammation than those without saline. Neither bleeding nor infection was observed at any site at any time. The electrode insertion sites treated with 4 and 5 V without saline showed blanched, yellow-white discoloration on days 0 and 1 (Fig. 3B,C,G,H). On day 7, the discoloration was replaced with redness (Fig. 3D,I), which largely resolved by day 14 (Fig. 3E,J). By day 29, redness disappeared for both the 4 and 5 V samples (Fig. 3F,K). On

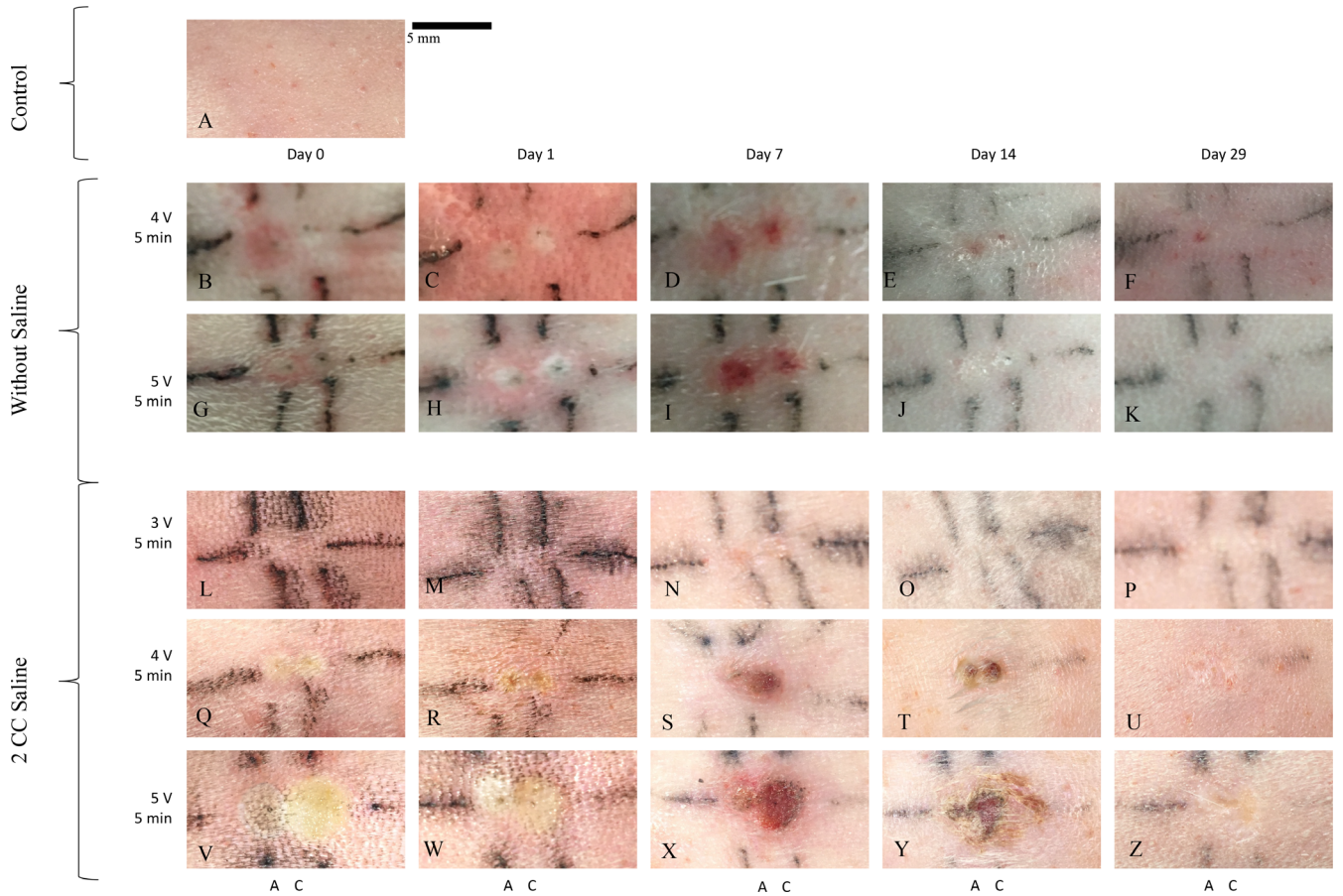

Fig. 3. Visible light photography of skin following electrochemical therapy (ECT). Following application of ECT, the surface of the dermal tissue was imaged with light photography over 29 days. Anodes and cathodes were placed 2 mm apart and denoted with A and C, respectively. The following treatments were applied: (A) control, (B–F) 4 V for 5 minutes without saline, (G–K) 5 V for 5 minutes without saline, (L–P) 3 V for 5 minutes with saline, (Q–U) 4 V for 5 minutes with saline, and (V–Z) 5 V for 5 minutes with saline. Vertical and horizontal tattoo lines were drawn to indicate electrode insertion sites. Scale bar indicates 5 mm.

days 0 and 1, tumescent tissue specimens treated with 3 V showed no discernible sign of superficial tissue change (Fig. 3L,M). By day 7, small areas of erythema became visible directly adjacent to the electrode insertion site (Fig. 3N). Erythema resolved by day 14 (Fig. 3O), and the skin appeared pristine at day 29 (Fig. 3P). Tumesced sites treated with 4 and 5 V developed a blanched, yellow-white hue on days 0 and 1, with the spatial area of this discoloration increasing with larger voltage (Fig. 3Q,V,R,W). By day 7, scabs appeared, surrounded by a region of erythema (Fig. 3S,X). By day 14, the erythema resolved (Fig. 3T,Y). Scabbing persisted through day 29 and fell off with removal of the occlusal dressing (Fig. 3U,Z). The skin previously covered by scabs was depressed and hypopigmented relative to the surrounding skin.

Ultrasound

High-frequency ultrasound images were acquired before and immediately after ECT and on postoperative days 1, 2, 3, 7, 14, and 29 (Fig. 4). The images were captured with a gel interface, and the image plane was parallel to the long axes of both anode and cathode needle

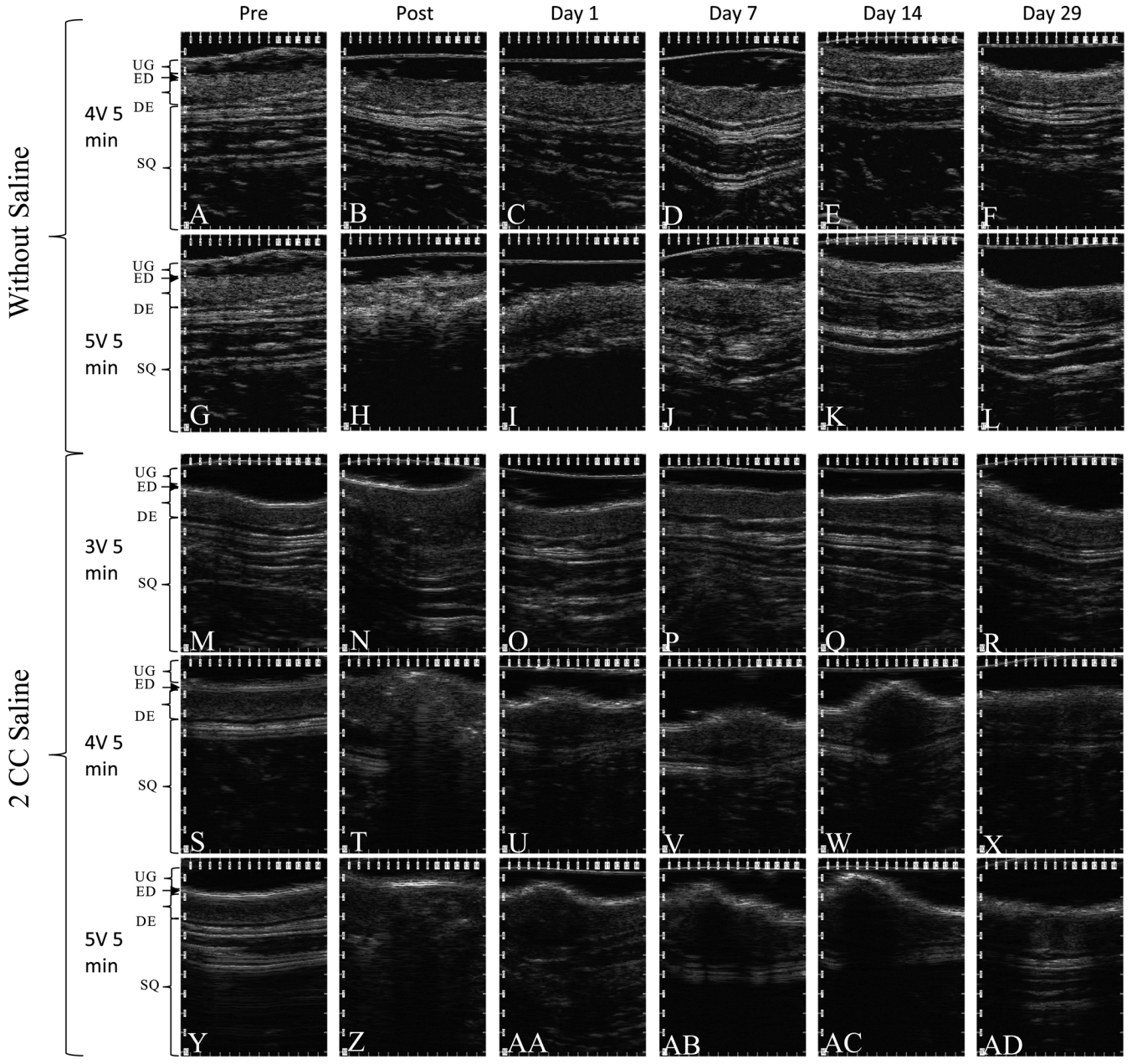

Fig. 4. High-frequency ultrasonography of skin following ECT. Following application of electrochemical therapy, the surface of the dermal tissue was imaged with high-frequency ultrasonography. The following treatment parameters were imaged: (A–F) 4 V for 5 minutes without saline, (G–L) 5 V for 5 minutes without saline, (M-R) 3 V for 5 minutes with saline, (S–X) 4 V for 5 minutes with saline, and (Y–AD) 5 V for 5 minutes with saline. The ultrasound images identify ultrasound gel (UG), epidermis (ED), dermis (DE), and subcutaneous tissue (SQ).

electrodes. Control imaging displayed clear demarcations between the layers of native rabbit skin, with the epidermis, dermis, and subcutaneous tissue readily identified (Fig. 4A,G,M,S,Y). In the images acquired immediately following ECT application, acoustic shadows were observed. This disruption increased in the dermis as the voltage increased (Fig. 4). In tissue treated without a saline injection, acoustic shadows were absent at 4 V but present at 5 V (Fig. 4B,H). In tumesced tissues, shadows were observed at all voltages (Fig. 4N,T,Z). The sites without saline injection imaged on days 1, 7, 14, and 29 (Fig. 4C,D, E,F,I,J,K,L) looked similar to controls (Fig. 4A,G). This was also observed with specimens treated with saline at 3 V (Fig. 4O,P,Q,R vs Fig. 4M). However, the 4 and 5 V sites with saline treatment showed swelling immediately post-treatment. Swelling for these conditions persisted on days 1, 7, and 14 along with a low-intensity acoustic signal under those regions (Fig. 4U,V,W,AA,AB,AC). On day 29, the swelling was absent, and a high-intensity signal was identified within the dermis (Fig. 4X,AD). This was not previously observed in controls (Fig. 4S,Y).

Histology

Histological analysis was performed on tissue samples after euthanasia on day 29 using H&E, MT, and PSR staining (Fig. 5). In controls, H&E stains indicated well-organized, thick, mature collagen and the presence of hair follicles, glandular structures, and blood vessels throughout (Fig. 5A,N). In the samples that were not injected with saline (Fig. 5B,C,H,I), an increased fibroblast density, along with inflammatory infiltrates, was observed, staining with a more intense blue hue due to increased hematoxylin uptake. Fine collagen fibers were observed as well. Collagen fibers were better visualized with MT staining (Fig. 5D,E,J,K). Collagen fibers in treated areas appeared thinner and less organized compared to the coarse, dark blue staining of more mature control tissue collagen. Increased cellularity and vascularity were also observed with the red Biebrich Scarlet component of the MT stain. A voltage of 4 V showed comparable changes in both electrodes, but at 5 V, these differences were more evident in the anode than in the cathode (Fig. 5H,I). Tissue changes at the 5 V anode were more intense than those seen at 4 V, and there was also an absence of hair follicles. The 5 V cathode sites showed discrete foci of fine collagen fibers with increased fibroblasts (Fig. 5J,K). Collagen fibers were further visualized with PSR staining to indicate the type of collagen present (Fig. 5F,G,L,M). At 4 V, treatment areas at both the anode and the cathode did not show a significant difference in the size of the collagen fibers (Figs. 5F,G). However, at 5 V, the treatment areas showed thinner collagen fibers at the treatment site as opposed to the intense red of the thicker, mature normal tissue (Figs. 5L,M). At both 4 and 5 V, the treatment sites showed similar ratios of red to green color as the surrounding untreated dermal tissue. Hair appeared as green.

Saline-injected samples at 3 V do not demonstrate any changes in collagen structure or adnexal composition, and both epidermal and dermal layers appeared similar to controls (Fig. 5O–T). For 4 V with saline, finer collagen fibers were observed at treatment sites (Fig. 5U,V), along with absent hair follicles and increased fibroblasts and small vessels. These findings were similar at both the anode and cathode, although the features were more diffuse with a larger footprint at the cathode. At 5 V with saline, this change was clearly evident and more

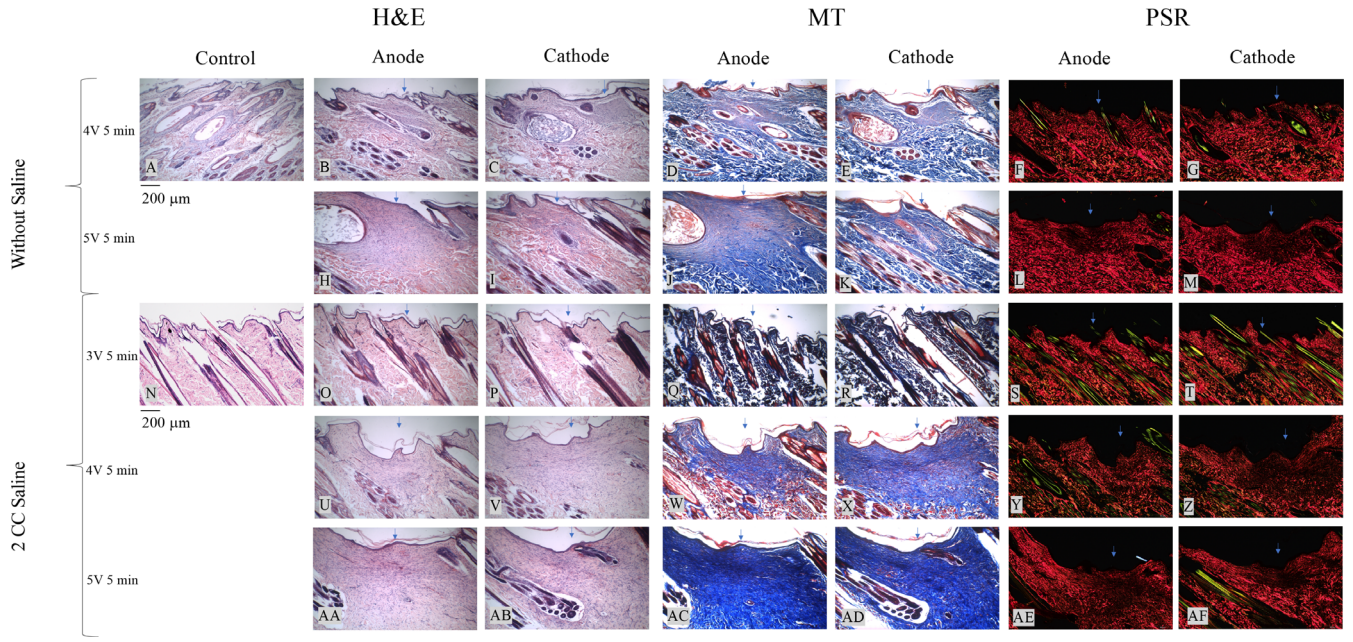

Fig. 5. Histological images of skin following electrochemical therapy. Histological Images of skin following ECT. Hematoxylin and Eosin (H&E)-, Masson's Trichrome (MT)-, and Picrosirius red (PSR)-stained histological images (10×) of skin samples at sites of control, anode, and cathode. The following treatment parameters were imaged: (A) control without saline, (B–G) 4 V for 5 minutes without saline, (H–M) 5 V for 5 minutes without saline, (N) control with saline, (O–T) 3 V for 5 minutes with saline, (U–Z) 4 V for 5 min with saline, and (AA–AF) 5 V for 5 minutes with saline. Scale bar indicates 200 µm. Arrows indicate electrode insertion site.

pronounced than at 4 V (Fig. 5AA,AB). The extent of tissue changes at the anode and cathode regions appear similar in size. Follicles were again absent. All of these changes were evidenced by the vibrant blue stain in MT staining (Fig. 5W,X,AC,AD). At 4 and 5 V, the treated areas showed thinner collagen fibers with the PSR stain, but the red to green color ratios appeared similar to that of the surrounding normal tissue (Fig. 5Y,Z,AE,AF).

DISCUSSION

Current minimally invasive technologies to treat scar, age-related changes, and sun damage may be expensive and require advanced training or skill. There exists an opportunity for a simple, low-cost method to remodel dermal collagen to potentially address these problems, particularly for hypertrophic scars and keloids. Here, we examined the effects of ECT in *in vivo* skin. Prior work by our group has shown that the effect is pH dependent and controllable with dosimetry.[2,24] We have further identified that tumescence can amplify the effect, and as most percutaneous procedures require some degree of local anesthetic, this finding is significant.

Although interstitial water content in the dermis is 70%,[35] saline injection was used to examine whether increased tissue water content and electrolytes could facilitate the ECT effect as water is the principal reagent undergoing electrolysis. Here, tumescence potentiated the ECT effect spatially. Without saline, hydrolysis might be limited by the diffusion of water as local concentrations are consumed during ECT. Saline may also increase the uniformity of the ECT effect and provide a more turgid structure through which to insert platinum-needle electrodes.

Photography of the surface showed that skin injury may occur during ECT, but the effect is localized, varying with dosimetry and the presence of injected saline. In the absence of tumescence, the visible effects of ECT on normal tissue were minimal, with no discernable changes observed at procedure sites on day 29 for both 4 and 5 V (Fig. 3F,K). This is of interest as the needles were not insulated and were in contact with the epidermis. The relatively low water content of the stratum corneum (15-40%) may be protective in this case, with little water to conduct current flow and undergo hydrolyis.[36] With saline, the visible area of effect increased with voltage. A voltage of 3 V showed no visible difference in treatment sites compared to control (Fig. 3P), suggesting that 3 V is the near-threshold value for ECT in skin. At 4 and 5 V, induction of electrolysis was evident by acute changes in tissue appearance and subsequent scab formation (Fig. 3Q,V,S,X). A voltage of 4 V created a smaller area of effect than 5 V, indicating dose dependence and the potential for precision therapy that would be necessary for skin rejuvenation procedures where damage must be spatially controlled. Scab formation at the surface may be prevented by insulating the electrode to the length of the epidermis, isolating ECT to the dermis, scar tissue, or keloid.

Ultrasonography demonstrated the subepidermal localization of the ECT effect (Fig. 4X,AD), confirmed by identification of new collagen on histologic sections. Electrodes penetrate tissue at a user-defined depth, allowing more spatial control than a chemical peel and with greater penetration depth into the dermis than lasers.[35] Ultrasonography identified acoustic shadowing after ECT application (Fig. 4H,N,T,Z) likely due to H_2 and O_2 gas formation—byproducts of hydrolysis.[2] This was not observed in specimens at 4 V in the absence of tumescence, indicating less gas evolution and, therefore, less hydrolysis (Fig. 4B). This suggests that 4 V without saline is a subtherapeutic parameter, unlike 5 V without saline, where acoustic shadows were observed (Fig. 4H). Ultrasonography of the skin over time did not identify significant change in tissue structure at either voltage (Fig. 4C,D,E, I,J,K), and on day 29, the structure of the skin resembled that of normal tissue. Tumesced tissue treated at 3 V appeared similar to the control immediately after ECT application, again suggesting subtherapeutic dosimetry (Fig. 4N), and no other changes were observed at later timepoints (Fig. 4O,P,Q). Acoustic shadows were evident in tumesced specimens at 4 and 5 V, with the extent increasing with voltage (Fig. 4T,Z). Inflammation was evident on days 1 to 14, indicated by the presence of swelling at treatment sites (Fig. 4U,V,W,AA,AB,AC). However, these sites also were affected by scabbing. A scab is dense tissue, and ultrasound images of these specimens provided limited information. By day 29, the scabs had fallen off, and ultrasonography was better able to penetrate deeper tissue composition (Fig. 4X,AD). The images on day 29 of saline-treated sites at 4 and 5 V revealed that higher-intensity signals followed the vertical path of the two electrodes. At 4 V (Fig. 4X), the signal was less intense and less spread out than at 5 V (Fig. 4AD). Christiansen et al. observed increased dermal density after laser skin rejuvenation treatment due to neocollagenesis.[37] As higher-intensity signals indicate denser tissue, this is suggestive of increased collagen deposition at treatment sites. Furthermore, the acoustic intensity increased with voltage, indicating a dose-dependent effect. Ultrasonography suggests that ECT induces localized and effective neocollagenesis.

Histology consistently identified localized dermal remodeling around electrode insertion sites. This suggests that tissue injury created by acid and base generation adjacent to the electrodes is followed by repair and wound healing. Increased fibroblast numbers and fine collagen fiber deposition indicate active neocollagenesis. The noticeably thinner collagen structures are characteristic of new collagen, in contrast to coarse, mature collagen bundles observed in the adjacent normal tissue. When examined for the presence of collagen type I versus type III, PSR indicated ratios similar to that of normal tissue. In rodent skin, collagen type I levels were shown to peak at 10 hours after injury and decrease to normal levels after 24 hours.[38] Furthermore, prolonged presence of increased levels of type III collagen is indicative of white or keloid scarring.[39] The similarity in color ratios in both treatment and normal areas, along with the evident thinner collagen fibers, indicate that neocollagenesis, as opposed to scarring, is occurring. Increased vascularity with inflammatory infiltrates suggests active neovascularization. Tumescent

samples showed an obvious difference between normal and ECT-treated tissues. Although 3 V continued to appear subtherapeutic (Fig. 5O–T), new collagen deposition was clearly observed at both 4 and 5 V (Fig. 5U–AF). These findings demonstrate that the ECT effect is localized based on needle geometry and dosimetry: as the voltage parameter increases, a subsequent increase in the area of effect is evident. This clearly underscores the importance of saline as it simultaneously serves as media for current flow and the principal reagent for hydrolysis. With the addition of saline, the histological effects of ECT are enhanced at both 4 and 5 V compared to native samples with the same voltage. Collectively, histology demonstrates that ECT focally injures tissue, followed by wound healing. This repair process is similar to that of deep chemical peels,[4] but the process is localized, allowing for possible precision in treatment. Spatial selectivity is, in turn, controlled by dosimetry, namely, voltage and application time and electrode design, which dictate the electric field geometry.

In chemexfoliation, acids are directly applied to skin, diffusing through the epidermis to denature proteins in the dermis, causing neocollagenesis.[3] The effect depends upon local tissue-diffusive properties, which vary considerably; operator skill and experience; and application time. In ECT, water is hydrolyzed, *in situ* acid and base evolve, and there is no need for drug injection or the costs of a laser or radiofrequency (RF) device. In contrast to a peel, penetration depth and lateral extent of the ECT process is controlled by dosimetry and needle geometry. Needle geometry controls the electric field, and this process can be feedback-controlled as well. No significant complications, such as gross tissue slough, muscle injury, etc., were observed during the 1-month duration of the study. However, in future studies, extending the evaluation period to 90 days would allow long-term observation of skin injury and repair. Furthermore, the current study examines the rejuvenation of normal tissue. Atrophic, hypertrophic, and keloid scarring is complex, and they can react varyingly to resurfacing treatments.[4,40] Finally, as a limited number of animals was studied, the results lack statistical power. Although ECT may demonstrate rejuvenation effects in normal tissue, its efficacy in scar tissue needs to be explored further.

CONCLUSION

Through light photography, ultrasound, and histological analyses, we have demonstrated that the electrolytic reaction of ECT induces localized regenerative dermal tissue. We have shown that the effect of ECT is dependent upon saline and the amount of water needed to produce localized acid/base. Although 3 V appears to have little effect, the application of 4 and 5 V dosages for a duration of 5 minutes reveal a parameter-dependent treatment with user-controlled depth penetration and lateral extent. Furthermore, ECT can prove to be a low-cost alternative to conventional treatments: the simplest construction of platinum-plated electrodes and a DC battery can cost approximately $10.[2] ECT can potentially offer precise, low-cost rejuvenation to restore the functionality and appearance of dermal scars and keloids.

ACKNOWLEDGMENTS

This research was supported by the Irvine Head and Neck Research Foundation, George Hewett Foundation, LAMMP Grant funded by the National Institutes of Health (NIH)/National Institute of Biomedical Imaging and Bioengineering (P41-EB015890), and the Leading Foreign Research Institute Recruitment Program through the National Research Foundation of Korea (NRF) funded by the Ministry of Science and ICT (NRF-2018K1A4A3A02060572). The content of the manuscript is solely the responsibility of the authors and does not necessarily represent the official views of the NIH.

BIBLIOGRAPHY

1. Kerwin L, El Tal A, Stiff M, TM F. Scar prevention and remodeling: a review of the medical, surgical, topical and light treatment approaches. *Int J Dermatol* 2014;53:922–936. https://doi.org/10.1111/ijd.12436.
2. Moy WJ, Su E, Chen JJ, et al. Association of electrochemical therapy with optical, mechanical, and acoustic impedance properties of porcine skin. *JAMA Facial Plast Surg* 2017;19:502–509. https://doi.org/10.1001/jamafacial.2017.0341.
3. Rendon MI, Berson DS, Cohen JL, Roberts WE, Starker I, Wang B. Evidence and considerations in the application of chemical peels in skin disorders and aesthetic resurfacing. *J Clin Aesthet Dermatol* 2010;3:32–43.
4. Deprez P. *Textbook of Chemical Peels, Second Edition: Superficial, Medium, and Deep Peels in Cosmetic Practice*. 2nd ed.: Boca Raton, FL: CRC Press; 2016.
5. Hurliman E, Zelickson B, Kenkel J. In-vivo histological analysis of a fractional CO_2 laser system intended for treatment of soft tissue. *J Drugs Dermatol* 2017;16:1085–1090.
6. Kim S, Manuel CT, Wong BJF, Chung PS, Mo JH. Handheld-level electromechanical cartilage reshaping device. *Facial Plast Surg* 2015;31:295–300. https://doi.org/10.1055/s-0035-1555623.
7. Hong SJ, Lee M, Oh CJ, Kim S. Monitoring of biological changes in electromechanical reshaping of cartilage using imaging modalities. *Biomed Res Int* 2016;2016:1–7. https://doi.org/10.1155/2016/7089017.
8. Oliaei S, Manuel C, Karam B, et al. In vivo electromechanical reshaping of ear cartilage in a rabbit model: a minimally invasive approach for otoplasty. *JAMA Facial Plast Surg.* 2013;15:34–38. https://doi.org/10.1001/2013.jamafacial.2.
9. Karlsmark T, Danielsen L, Thomsen HK, et al. Ultrastructural changes in dermal pig skin after exposure to heat and electric energy and acid and basic solutions. *Forensic Sci Int* 1988;39:235–243. https://doi.org/10.1016/0379-0738(88)90126-0.
10. Ho KHK, Valdes SHD, Protsenko DE, Aguilar G, Wong BJF. Electromechanical reshaping of Septal cartilage. *Laryngoscope* 2003;113:1916–1921. https://doi.org/10.1097/00005537-200311000-00011.
11. Yau AYY, Manuel C, Hussain SF, Protsenko DE, Wong BJF. In vivo needle-based electromechanical reshaping of pinnae New Zealand white rabbit model. *JAMA Facial Plast Surg.* 2014;16:245–252. https://doi.org/10.1001/jamafacial.2014.85.
12. Tracy LE, Wong BJ. The effect of pH on rabbit septal cartilage shape change: exploring the mechanism of electromechanical tissue reshaping. *Eplasty* 2014;14:e23. http://www.pubmedcentral.nih.gov/articlerender.fcgi?artid=PMC4080822.
13. Hussain S, Manuel CT, Protsenko DE, Wong BJF. Electromechanical reshaping of ex vivo porcine trachea. *Laryngoscope* 2015;125:1628–1632. https://doi.org/10.1002/lary.25189.
14. Badran KW, Manuel CT, Loy AC, et al. Long-term in vivo electromechanical reshaping for auricular reconstruction in the New Zealand white rabbit model. *Laryngoscope* 2015;125:2058–2066. https://doi.org/10.1002/lary.25237.
15. Manuel CT, Tjoa T, Nguyen T, Su E, Wong BJF. Optimal electromechanical reshaping of the auricular ear and long-term outcomes in an in vivo rabbit model. *JAMA Facial Plast Surg* 2016;18:277–284. https://doi.org/10.1001/jamafacial.2016.0166.
16. Manuel CT, Foulad A, Protsenko DE, Hamamoto A, Wong BJF. Electromechanical reshaping of costal cartilage grafts: a new surgical treatment modality. *Laryngoscope* 2011;121:1839–1842. https://doi.org/10.1002/lary.21892.
17. Protsenko DE, Ho K, Wong BJF. Stress relaxation in porcine septal cartilage during electromechanical reshaping: mechanical and electrical responses. *Ann Biomed Eng* 2006;34:455–464. https://doi.org/10.1007/s10439-005-9051-y.
18. Manuel CT, Foulad A, Protsenko DE, Sepehr A, Wong BJF. Needle electrode-based electromechanical reshaping of cartilage. *Ann Biomed Eng* 2010;38:3389–3397. https://doi.org/10.1007/s10439-010-0088-1.
19. Protsenko DE, Ho K, Wong BJF. Survival of chondrocytes in rabbit septal cartilage after electromechanical reshaping. *Ann Biomed Eng* 2011;39:66–74. https://doi.org/10.1007/s10439-010-0139-7.

20. Wu E, Protsenko DE, Khan AZ, Dubin S, Karimi K, Wong BJF. Needle-electrode-based electromechanical reshaping of rabbit septal cartilage: a systematic evaluation. *IEEE Trans Biomed Eng* 2011;58:2378–2383. https://doi.org/10.1109/TBME.2011.2157155.
21. Protsenko DE. Changes in the tangent modulus of rabbit septal and auricular cartilage following electromechanical reshaping. *J Biomech Eng* 2011; 133:094502. https://doi.org/10.1115/1.4004916.
22. Kuan EC, Hamamoto AA, Manuel CT, Protsenko DE, Wong BJF. In-depth analysis of pH-dependent mechanisms of electromechanical reshaping of rabbit nasal septal cartilage. *Laryngoscope* 2014;124:E405–E410. https://doi.org/10.1002/lary.24696.
23. Badran K, Manuel C, Waki C, Protsenko D, Wong BJF. Ex vivo electromechanical reshaping of costal cartilage in the New Zealand white rabbit model. *Laryngoscope* 2013;123:1143–1148. https://doi.org/10.1002/lary.23730.
24. Hu AC, Hong EM, Toubat O, et al. Multiphoton microscopy of collagen structure in ex vivo human skin following electrochemical therapy. *Lasers Surg Med* 2019;52:196–206. https://doi.org/10.1002/lsm.23094.
25. Hunter BM, Kallick J, Kissel J, et al. Controlled-potential electromechanical reshaping of cartilage. *Angew Chem Int Ed* 2016;55:5497–5500. https://doi.org/10.1002/anie.201600856.
26. Jayaraman V, Jiang J, Potsaid B, Cole G, Fujimoto J, Cable A. Design and performance of broadly tunable, narrow line-width, high repetition rate 1310 nm VCSELs for swept source optical coherence tomography. *SPIE*. 2012;8276:1–11. https://doi.org/10.1117/12.906920.
27. Qu Y, Ma T, He Y, et al. Acoustic radiation force optical coherence Elastography of corneal tissue. *IEEE J Sel Top Quantum Electron* 2016; 22:0–18. https://doi.org/10.1109/JSTQE.2016.2524618.
28. Liang X, Boppart S. Biomechanical properties of in vivo human skin from dynamic optical coherence Elastography. *IEEE Trans Biomed Eng* 2013; 57:953–959. https://doi.org/10.1109/TBME.2009.2033464.Biomechanical.
29. Gambichler T, Jaedicke V, Terras S. Optical coherence tomography in dermatology: technical and clinical aspects. *Arch Dermatol Res* 2011;303: 457–473. https://doi.org/10.1007/s00403-011-1152-x.
30. Pagnoni A, Knuettel A, Welker P, et al. Optical coherence tomography in dermatology. *Ski Res Technol* 1999;5:83–87. https://doi.org/10.1117/1.JBO.18.6.061224.
31. Kong L, Caspall J, Duckworth M, Sprigle S. Assessment of an ultrasonic dermal scanner for skin thickness measurements. *Med Eng Phys* 2008;30: 804–807. https://doi.org/10.1016/j.medengphy.2007.10.002.
32. Rolls GO, Tarbet F, Scott-Dowell K, Hopkins A, Farmer N, Taggart G. *Difficult Blocks and Reprocessing*. Melbourne, Australia: Leica Microsystems; 2011.
33. Flint MH, Lyons MF. The effect of heating and denaturation on the staining of collagen by the Masson trichrome procedure. *Histochem J* 1975;7: 547–555. https://doi.org/10.1007/BF01003792.
34. Montes GS, Junqueira LCU. The use of the Picrosirius-polarization method for the study of the biopathology of collagen. *Mem Inst Oswaldo Cruz* 1991;86:1–11.
35. Waibel JS, Rudnick A. Laser-assisted delivery to treat facial scars. *Facial Plast Surg Clin North Am* 2017;25:105–117. https://doi.org/10.1016/j.fsc.2016.08.010.
36. Warner RR, Myers MC, Taylor DA. Electron probe analysis of human skin: determination of the water concentration profile. *J Invest Dermatol* 1988; 90:218–224. https://doi.org/10.1111/1523-1747.ep12462252.
37. Christiansen K, Bjerring P. Low density, non-ablative fractional CO2 laser rejuvenation. *Lasers Surg Med* 2008;40:454–460. https://doi.org/10.1002/lsm.20660.
38. Clore JN, Cohen IK, Diegelmann RF. Quantitation of collagen types I and III during wound healing in rat skin. *Proc Soc Exp Biol Med* 1979;161: 337–340. https://doi.org/10.3181/00379727-161-40548.
39. Sunaga A, Kamochi H, Sarukawa S, et al. Reconstitution of human keloids in mouse skin. *Plast Reconstr Surg Glob Open* 2017;5:1–7. https://doi.org/10.1097/GOX.0000000000001304.
40. Baumann ME, Blackstone BN, Malara MM, et al. Fractional CO_2 laser ablation of porcine burn scars after grafting: is deeper better? *Burns* 2019; 46:1–12. https://doi.org/10.1016/j.burns.2019.10.009.